Agenzia nazionale per le nuove tecnologie,
l'energia e lo sviluppo economico sostenibile

MINISTERO DELLO SVILUPPO ECONOMICO

Ricerca di Sistema elettrico

# Sviluppo di una configurazione di plasma di tipo "Snow-Flake" FAST-like per EAST

F. Crisanti, G. Calabrò, G. Ramogida

G. Di Gironimo, R. Albanese, R. Ambrosino

Report RdS/PAR2013/220

# SVILUPPO DI UNA CONFIGURAZIONE DI PLASMA DI TIPO “SNOW-FLAKE” FAST-LIKE PER EAST

F. Crisanti, G. Calabró, G. Ramogida (ENEA)
G. Di Gironimo, R. Albanese, R. Ambrosino (CREATE Napoli)

Settembre 2014

Report Ricerca di Sistema Elettrico
Accordo di Programma Ministero dello Sviluppo Economico – ENEA
Piano Annuale di Realizzazione 2013
Area: Produzione di Energia Elettrica e Protezione dell’Ambiente
Progetto: B.3.2 Attività di fisica della Fusione complementari a ITER
Obiettivo: FAST il nuovo esperimento satellite europeo
Responsabile del Progetto: Aldo Pizzuto, ENEA

# Index

# Summary

Heat and particle loads on the plasma-facing compents are the most challenging points to be solved for a reactor design. The quasi snowflake (QSF) divertor is an alternative magnetic configuration that may enable tokamak operation at lower peak heat load than a standard single-null (SN) divertor. Recently this magnetic divertor configuration has been studied and proposed for the planned FAST Tokamak and for the demonstrative Power Plant DEMO. In this report we illustrate how a QSG configuration has been studied and eventually realized on the EAST tokamak. Differently of what could happen on FAST and DEMO, EAST does not have poloidal coils optimized to realize such a configuration. However, EAST have only 12 independent poloidal field coils (PFCs) to shape the plasma and, eventually, to realize QSF configuration, even if not at the highest plasma currents achievable on EAST. The first experimental results confirm the divertor geometric proprieties of the simulated QSF configuration. QSF configurations have been designed and optimized by CREATE-NL tools, the same tools used for the FAST and DEMO proposals, these studies will be discussed in this report. Predictive edge simulations by using the code TECXY will also be presented by comparing the QSF and SN configurations and compared with the preliminary experimental results on the power loads on the divertor tiles.

# 1 Introduction

Heat and particle loads on the plasma-facing components are the most challenging points to be solved for a reactor design [1]. In ITER, mitigation by radiative dissipation of the exhaust power may still be adequate. However, present scaling of the scrape-off layer (SOL) width [2] extrapolates to unmitigable heat fluxes in reactor-scale machines with conventional divertor geometry, i.e. an axisymmetric magnetic X-point. One approach to handling the high exaust power on plasma face components is to use alternative magnetic configurations, such as the Super X-divertor [3,4] and Snowflake Divertor (SFD) [5]. A Snow Flake (SF) configuration is characterized by a second-order null (x-point) in the poloidal magnetic field ($B_p$), where both $B_p$ itself and its spatial derivatives vanish ($B_p = 0$, $\nabla B_p = 0$). This splits the separatrix near the null into six segments: two enclose the confined plasma and four lead to the machine wall (the divertor legs). The poloidal cross-section of the obtained magnetic flux surfaces with a hexagonal null-point has an appearance of a snowflake. Theoretical studies indicate that the SF magnetic geometry leads to both higher power losses during SOL transport and an increased plasma wetted area of the wall [6]. The former results from an increase in the connection length and the divertor volume, the latter from an increase in flux expansion and SOL width, and from the doubling of the number of strike points (SPs) compared with the conventional X-point divertor configuration. The first SF was experimentally established on TCV in 2009 [7], and later on the spherical tokamak NSTX [8] and finally in the larger tokamak DIII-D [9].

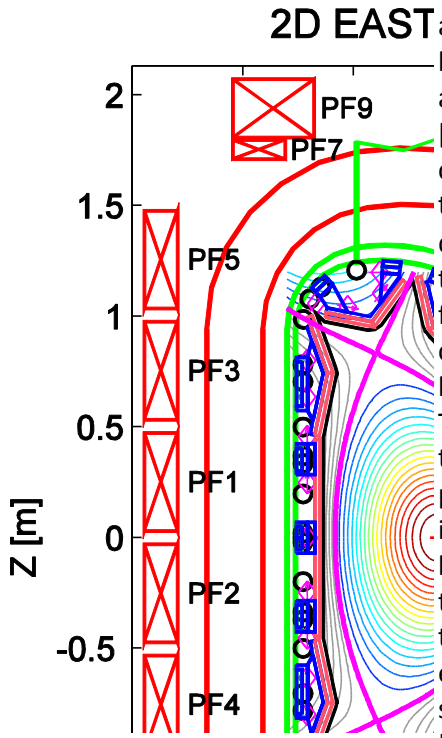


**Figure 1. Two-dimensional EAST geometry schematic view.**

This Chinese Experimental Advanced Superconducting Tokamak (EAST) presents several advantages in studying the integrated bulk-edge Power Exhaust (P-EX) problem. It is steady state; it has a actively cooled divertor in Tungsten, using the same monoblocks technology that will be used in DEMO; it has a large power density and power flux on the divertor tiles; eventually, having all the pololidal coils independently fed, the possibility to realize QSF configurations. As shown in Fig. 1, EAST is constructed to be up-down symmetric, with the following main parameters [10]: major radius R = 1.8 m, minor radius a = 0.45 m, toroidal field $B_T$ up to 3.5 T, and plasma current $I_p$ up to 1 MA for highly elongated plasma elongation $\kappa$ = 1.9. It can be operated in quite flexible plasma shapes with an elongation factor $\kappa$ = 1.5-2.0 and triangularity $\delta$ = 0.3-0.6 for double null (DN) or single null (SN) divertor configurations. EAST is equipped with 14 superconducting poloidal field coils (PFCs) for ohmic heating, ohmic current drive, shaping and position control [11]. It should be noted that PFCs 7 and 9 are connected in series as are PFCs 8 and 10. Thus, there are in total 12 independent PF power supplies (max current IPF = 14.5kA). EAST also has in-vessel active feedback coils (IC coils) for fast control of the plasma vertical instability; they consist of two 2-turn coils symmetrically located in the upper and lower part of the vessel and connected in new very and, has with

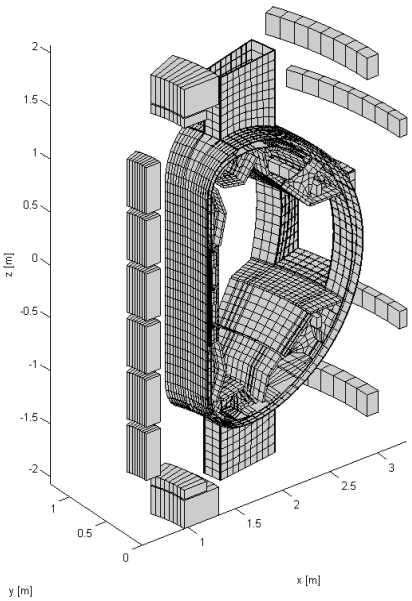


**Figure 2. Details of the 3D mesh used for vertical stability analyses.**

anti-series in order to provide an horizontal field. An exact SF constistues a single null point in the magnetic configurations space. As was realized in the first assessments of SF [6] an exact snowflake configuration is topologically unstable: either by choice or due to the fact that PF coil currents are slightly different from the exact value and/or pertubations of the magnetic equilibrium caused e.g. by plasma instabilities, the second-order null is split in two first-order nulls (x1, x2) leading to so-called Quasi Snowflake configurations (QSF). The distance between the two x-points, i.e. the proximity to the exact SF [12], is parametrized by the dimensionless parameter $\sigma$ = D/*a*, with D the x-point separation and *a* the plasma minor radius. The position of x2 relative to x1 determines the local geometry of the null region and hence the properties of the divertor.

# 2 Description of activities and results

## *2.1 EAST snowflake equilibria optimization.*

QSF configurations (for FAST, DEMO and as well EAST) have been designed and optimized by means of CREATE-NL code (non linear plasma evolution code), described in [13], in combination with EFIT [14] and FIXFREE [15] static equilibrium codes. The tokamak simulation code (TSC) [16], a numerical model of the axisymmetric tokamak plasma and the associated control systems, has been then used to model the EAST QSF full plasma scenario. TSC outputs have been finally used to set the Plasma Control Systems (PCS) operating during the experiments. The procedure proposed for the design and optimization of QSF configurations by CREATE-NL code exploits the linearized relation between the plasma-wall gaps and the PF currents [17]. It composed by two-step: i) the first step allows to have a first cut of the QSF equilibrium starting from a standard single null plasma configuration: a new equilibrium with a second null point within a limited distance from SN x-point is obtained, forcing the plasma boundary to be almost unchanged, apart from the region in the vicinity of the null point; ii) the second step refines the plasma shape and possibly reduces the PF coil currents while fulfilling the machine technological constraints. For EAST, QSF equilibria are identified as modifications of experimental reference SN discharge #43362 ($I_P \sim 400$kA, $B_T = 1.8$T, internal plasma inductance $l_i \sim 1.4$, poloidal beta $\beta_p \sim 0.1$) with the following constraints to be verified: a) coil currents $I_k$ far enough from their limits: $I_{min} + \Delta I \le I_k \le I_{max} - \Delta I$, with $\Delta I = 0.1 \max\{|I_{min}|, |I_{max}|\}$; b) vertical instability growth rate not much larger than reference SN configurations; c) strike points on vertical targets; d) at least 20 mm clearance (gap) between plasma boundary and first wall. The objectives of the QSF design and optimization procedure consists in the definition of a set of QSF configurations, at low and high $\beta_p$ with the second null close ($\sigma \sim 0.84$) and far ($\sigma \sim 1.87$) from the vessel structures maximizing the

| | QSF low $\beta_p$ 400kA "close nulls" | QSF high $\beta_p$ 400kA "close nulls" | QSF low $\beta_p$ 480kA "far nulls" | QSF high $\beta_p$ 480kA "far nulls" | Reference SN_43362 |
|---|---|---|---|---|---|
| **$I_P$ [kA]** | 400 | 400 | 480 | 480 | 388 |
| **$\beta_p$** | 0.1 | 0.45 | 0.1 | 0.45 | 0.1 |
| **$l_i$** | 1.4 | 1.4 | 1.4 | 1.4 | 1.26 |
| **κ** | 1.73 | 1.72 | 1.71 | 1.71 | 1.65 |
| **Volume [m^3]** | 12.21 | 12.59 | 12.28 | 12.76 | 11.02 |
| **Flux Expansion $f_m$** | 58.72 | 53.52 | 19.85 | 21.60 | 3.54 |
| **Connection length L (m)** | 129.74 | 126.23 | 103.50 | 101.47 | 94.93 |
| **Growth rate lower bound [$s^{-1}$]** | 186 | 161 | 148 | 120 | 88 |
| **Growth rate upper bound [$s^{-1}$]** | 474 | 339 | 341 | 241 | 195 |
| **Growth rate [$s^{-1}$]** | 132 | 112 | 103 | 78 | 61 |
| **Stability margin** | 0.46 | 0.52 | 0.55 | 0.66 | 0.86 |

**Table I. EAST optimized QSF configurations by CREATE-NL code**

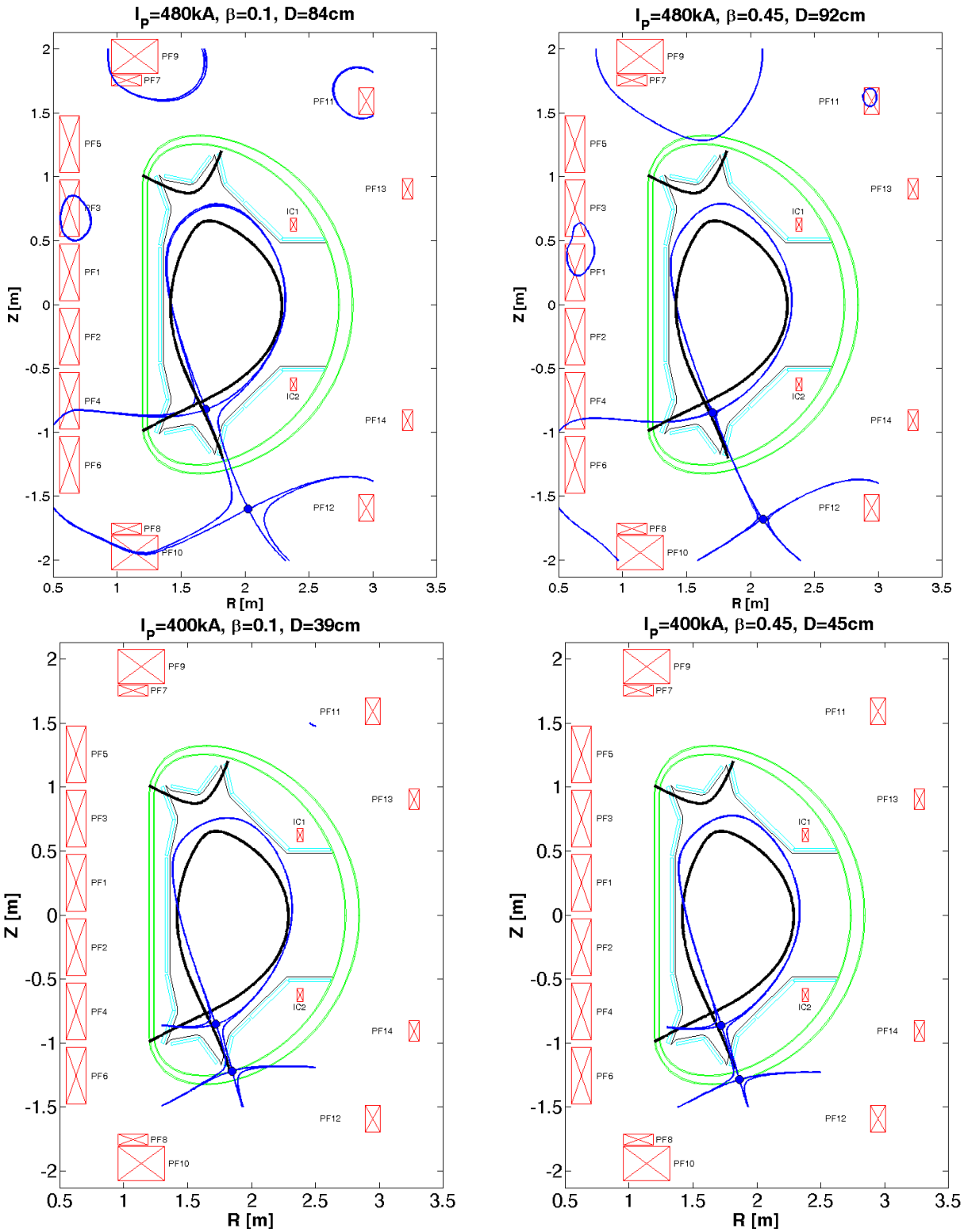


**Figure 3. Plasma boundary of optimized QSF equilibria (blue solid line) at low and high beta compared to the reference SN experimental boundary (black solid line) calculated by CREATE-NL code. Also the x-point separation D is reported for alle the QSF equilibria.**

plasma current. The vertical stability analyses have been carried out with reference to the passive structures. Detailed comparison of model predictions with the experimental results with reference to Vertical Displacement Events (VDEs) for three configurations with typical high (≈366 s-1), medium (≈229 s-1) and low (≈98 s-1) growth rates are reported in [18]. Fig. 2 shows some details of the 3D mesh used for

vertical stability analyses. The optimized QSF configurations obtained with CREATE-NL and then verified by EFIT and FIXFREE code are summarized in Table 1. Also typical geometry factors as connection length *L* and poloidal magnetic flux expansion $f_m$, [12] in the outer SP region, are reported. The simulated QSF and experimental reference SN equilibria are shown in Fig. 3. For the QSF configurations with $I_P$=400 kA the second x-point is located on the vessel (on the inner shell at low beta, on the outer shell location for a high beta plasma) as shown in Fig. 3. However, the second null point may be brought inside the vessel at the price of a lower plasma current or a higher plasma elongation. We can also observe that: 1) high poloidal beta configuration is more demanding in terms of PF currents and presents larger x-point separation D; 2) on the other hand the “close nulls” QSF equilibria present higher flux expansion on the divertor plates, and SOL in its throat on the plates. However, the plasma current for these configurations is of 400kA lower than the 480kA of “far nulls” case.

## 2.2 Predictive QSF SOL plasma simulations".

Predictive edge simulations of the standard SN divertor and QSF configurations have been run with the flexible, quick and versatile multifluid 2D edge code TECXY [19]. TECXY takes into account all the main physics processes, atomic and plasma, occurring into the scrape off layer (SOL), but the neutral dynamics, i.e. generation of atoms at the solid surfaces and transport into the SOL, is treated with an analytical model instead of the more rigorous Monte Carlo method. This ensures a rapid convergence to a steady state and makes the code very useful for exploring a wide range of the operational parameter space. Conversely, the plasma status when it is detached from the divertor target cannot be reliably detailed, but only the approach to such conditions can be outlined. The code validity has been successfully checked on several experimental data of [19, 20]. On EAST and FAST we used TECXY as a tool for comparing the SN and QSF configurations in terms of the SOL global power losses and of the load profiles on the targets, over the operational plasma density range. The parameters considered in the EAST simulations so far are: outboard density at separatrix $1.5 \le ne_{sep} \le 4.2 \times 10^{19}$ $m^{-3}$, corresponding roughly to the line averaged density range 3.5-10 $\times 10^{19}$ $m^{-3}$, power input into the SOL PSOL = 3MW, plasma current $I_P$ = 0.3kA and $B_T$ = 1.8T. No impurity has been at present still considered. On going are the widening of the explored parameter space and the data analysis for the QSF configuration only very recently actually realized. In Fig.4 the total power deposited on both (inner and outer) divertor plates for SN and QSF is plotted versus the plasma density at the outboard midplane. The QSF curve is always below the SN one, i.e. the total volume losses are higher. As already found in the code runs for FAST [21, 22] the load mitigating properties of the QSF are exalted at higher density. Indeed, a further significant drop for the QSF total load is found for $ne_{sep} \ge 2.5 \times 10^{19}$ $m^{-3}$ in EAST. According to the previous studies the main physics mechanism responsible for the higher QSF volume losses should be the much longer magnetic connection lengths. This prolongs the particle dwell time inside the SOL so that the number of interaction with the background neutrals during the particle lifetime increases and the energy losses are enhanced. Quite contemporary to the divergence of the two curves, the features of plasma detachment are expected to appear. Indeed just at that value of $ne_{sep}$, the plot of the peak power load on the outer target for SD and QSF, in Fig.5, shows a clear change in the slope for QSF, sign of an efficient shielding of the plate. No significant change is instead observed for SD, whose values are divided by 10 in the figure for facilitating the comparison. It has to be noted for the sake of clarity that these loads correspond to targets perpendicular to the poloidal field: the actual values should take into account the real inclination of the plates. Validation to these results comes from the case so far considered also with EDGE2D [23], where the actual divertor geometry is considered and the neutrals dynamics is treated with a Monte Carlo computing technique.

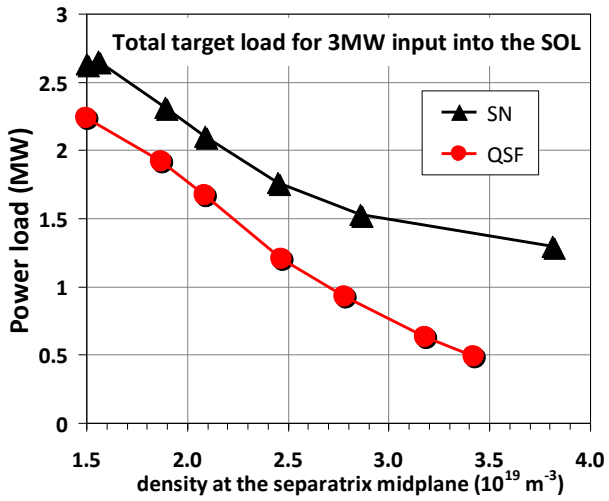


**Figure 4. Total load on both targets versus the plasma density at the outboard midplane. The power input into the SOL is 3.0 MW.**

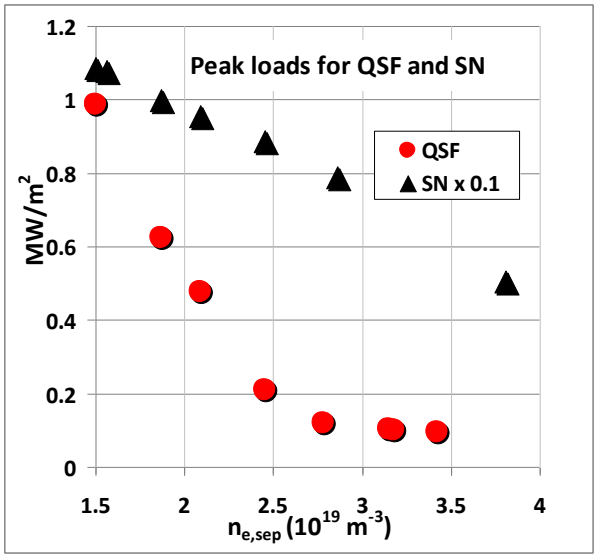


Figure 5. Peak power load onto the outer target versus the plasma density at the outboard midplane for both standard (SN) and quasi snow flake (QSF) divertor.

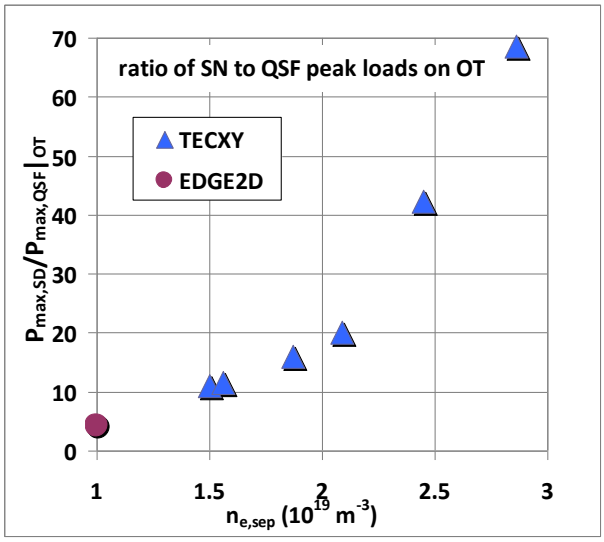


Figure 6. QSF peak mitigation factor, as derived from TECXY and EDGE2D runs. The point from this last code aligns very well to the others, despite the very different calculation method.

This is shown in Fig.6 where we plot the ratio (SD to QSF) between the peak values of the loads onto the outer target versus the density at separatrix on the outboard equator. The point at the lowest density, derived from EDGE2D, is clearly the prolongation of the curve obtained from TECXY runs. This picture also clear shows how strong can be the mitigation of the peak deposition power, as combination of the flux expansion, which dominates at low density, and of the enhanced dissipation processes, which dominates at the higher densities. Again it is visible a change in the slope close to $ne_{sep}=2.5\times10^{19}$ $m^{-3}$ that should be attributed to the start of detachment. The deposition profiles on to the outer divertor target are finally presented in Fig.7 for two working plasma densities, $ne_{sep}=1.5$ and $2.1\times10^{19}$ $m^{-3}$, which lie inside the range of full reliability of TECXY. For the higher density this figure not only details for QSF the large improved mitigation of the peak power, but also clearly puts into evidence how the load smears out over a longer distance and the peak position is slightly outwards shifted. Neither of the two last features is present in SD curves. The second one (i.e. the peak shift) is the first hint of detachment. We can summarize the predictive work with TECXY saying that a lot of benefit, in term of the power load onto the divertor, is expected from changing the divertor magnetic configuration form the standard to the quasi snow flake configuration. Consistency is found with previous simulations with EDGE2D. The mitigation apparently improves at the highest densities, as found in other papers, and should be particularly evident with high additional heating power, since a stronger absolute drop of the loads has to develop for the same mitigation factor.

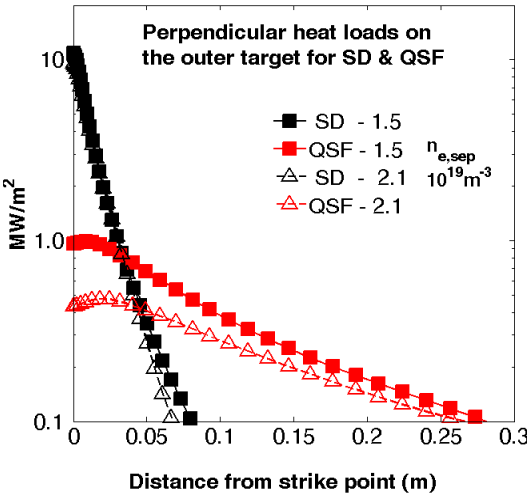


Figure 7. Power deposition profiles on to the outer target for two densities at separatrix for QSF (in red) and SD (in black). The target is set perpendicular to the poloidal field in the simulation.

## 2.3 Experimental results.

A First EAST QSF experiments have been lately performed, after a major upgrades where the upper divertor has been changed by installing an ITER-like W monoblock configuration with up to 10MW/m$^2$ heat removing capacity. In these experiments the simplest form of plasma current and position (i.e. plasma centroid) control has been used, the so-called RZIP control [11]. The control parameters are regulated by adjusting the current in PF coils. The requested PF coil current is composed of the sum of feed-forward (FF) and feedback (FB) components. The adaptation of the more sophisticated EAST ISOFLUX shape controller [24] to QSF configuration is still ongoing. The PFC currents discussed in the previous Section has been used as FF component target in RZIP control for QSF experiments (here only far nulls case). Magnetic and plasma characteristics of QSF have been studied in discharges with $I_P$ = 0.25MA and $B_T$ = 1.8T, $\kappa$ = 1.79, $q_{95} \sim 8$, $\kappa \sim 1.8$, ohmic and with 0.4MW of NBI heating.

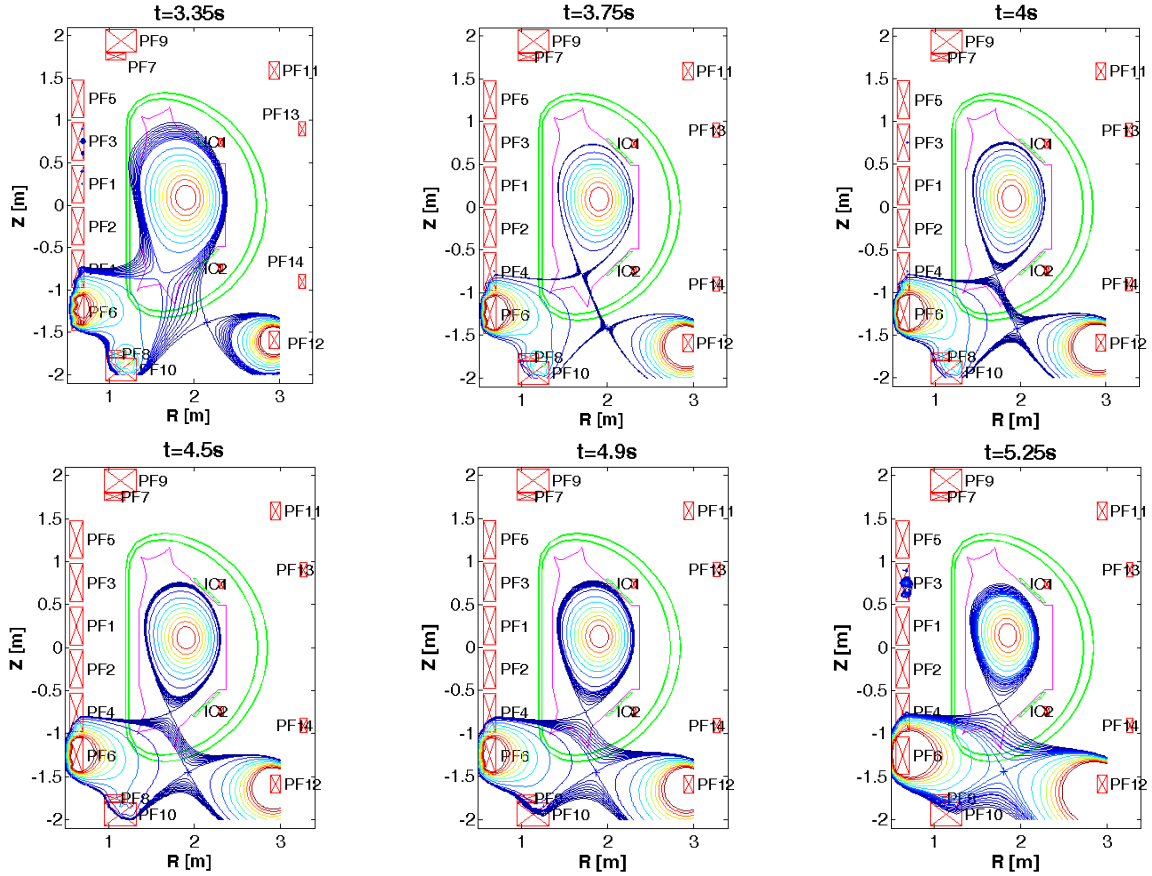


**Fig. 8. Sequence of EFIT reconstructd equilibria for ohmic QSF discharge #47660 from 3.35 to 5.25s.**

Fig. 8 shows the experimental magnetic equilibria at different time, reconstructed with Grad-Shafranov equilibrium code EFIT using standard magnetic and kinetic constraints for ohmic discharge #47660. It should be noted that the secondary null point is moving during the discharge. This observation indicates that a real time active divertor-null point separation control could be studied and then implemented in EAST PCS. Two L-mode discharges with similar PSOL≈0.3MW, but with different configurations (the standard divertor SN versus the QSF) will be compared. In Fig.9 the EFIT reconstructed equilibria for QSF #48971 (at t=4.5s, with $\beta_{pol}$ = 0.766 and $l_i$ = 1.283) and SN #47038 (at t=4.5s, with $\beta_{pol}$ = 0.584 and $l_i$ = 1.564) discharges are shown. Also the low-divertor Langmuir Probes (LPs) arrays are shown. Experimental magnetic geometry properties for both configurations are compared in Table II. These results confirm the predictions discussed in the previous section: the presence of a secondary null-point in QSF reduces $B_p/B_{tot}$ in the divertor separatrix region, where $B_{tot}$ is total magnetic field, and this increases the connection length

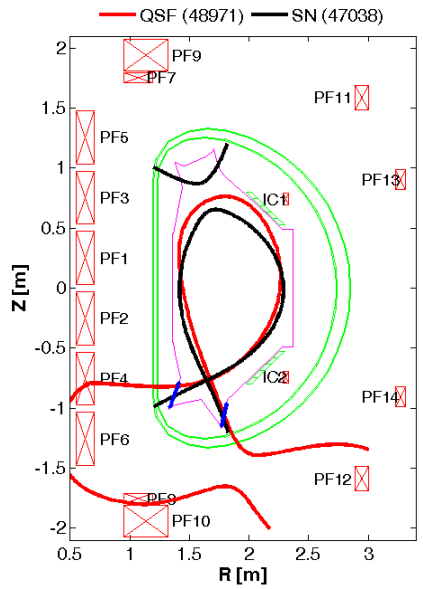


**Figure 9. Schematic 2D view of EAST with SN #47039 at t=4.5s (black solid line) and QSF (red solid line) at t=4.5s plasma boundaries. The x-point separation *D* is = 79cm for the QSF discharge. Also the low-divertor LPs arrays (blue solid points) are shown: inner LI01..15 and outer LO01…LO20 probes.**

**Table II. Main magnetic geometry properties for SN and QSF configurations, assuming SOL width at midplane of 2mm.**

| | **QSF**, #48971 at t=4.5s | **SN**, #47038 at t=4.5s |
|---|---|---|
| SOL Volume [$m^3$] | 0.389 | 0.260 |
| Connection Length [m] | 189.91 | 144.38 |
| Magnetic flux expansion at outer SP $f_{m,out}$ | 14.39 | 3.64 |
| Magnetic field angle at outer SP $\alpha_{out}$ [deg] | 0.469 | 2.17 |
| Magnetic flux expansion at inner SP $f_{m,in}$ | 5.21 | 3.47 |
| Magnetic field angle at inner SP $\alpha_{in}$ [deg] | 0.419 | 1.35 |

by ~30% and the flux expansion in the outer SP region by a factor ~5. The experimental connection length is higher than the predictive one of a factor ~1.5, for both QSF and SN, as expected due to the fact that the experimental $I_P$ is ~45% lower than the simulated one. Time evolution of main plasma quantities for SN and QSF discharge are shown in Fig.10: plasma current $I_P$, line avarage electron density ne, additional heating $P_{HEAT}$ (Lower Hybrid (LH) and NBI power respectively for #47038 and #48971), $q_{95}$ and elongation $\kappa$. It should be noted that from ~4.3sec the QSF configuration becomes stable. Preliminary spatio-temporal profiles of the ion saturation current density $j_{SAT}$ for both QSF and SN discharges are shown in Fig. 11. Only inner and outer low-divertor LPs arrays are considered in this study. A first qualitative observation indicates that in discharge #48971, once the QSF configuration becomes stable, the peak of $j_{SAT}$ drastically drops. In SN discharge #47038, even if the particle fluxes to SPs are minor than QSF #48971 case, both inner and outer are quite active during all the discharge. Further LPs data analysis with interpretative edge simulations are needed to quantify and explain a possible heat flux reduction.

# 3 Conclusioni

First quasi snowflake divertor configuration have been designed and simulated for FAST and EAST; for the last, the simulations have lately been verified by the experiemnts been experimentally. It has been demonstrated that a QSF plasma may be obtained without dedicated divertor coils and with a number of PFCs compatible with new experiments like JT60-SA and the design of the DEMO Power Plant. The results confirm the predictions of the designed QSF configurations, that have been optimezd by the CREATE-NL tools: the presence of a secondary null-point in QSF reduces $B_p/B_{tot}$ in the divertor separatrix region, where $B_{tot}$ is total magnetic field, and this increases the connection length by ~30% and the flux expansion in the outer SP region by a factor ~5. These first experiments also indicate that the plasma current could be increased (all the PFC currents are ~30% lower the limit) and that the distance between the two x-points $\sigma$ in the QSF configuration could be further reduced in order to investigate at what $\sigma$ the QSF behaves as an exact SF in terms of exhaust properties. It has been experimentally observed that in L-mode discharge the peak of ion saturation current density in LPs drops once the QSF configurations becomes stable compared to a SN case, that could indicate a heat flux reduction. Further data analysis and edge simulations are needed to verify and explain this experimental observation. Finally, predictive edge simulations highlighted the benefit, in term of the power load onto the divertor, that are expected from changing the divertor magnetic configuration form SN to the QSF configuration. The mitigation apparently improves at the highest densities, as found in other papers, and should be particularly evident with high additional heating power, since a stronger absolute drop of the loads has to develop for the same mitigation factor.

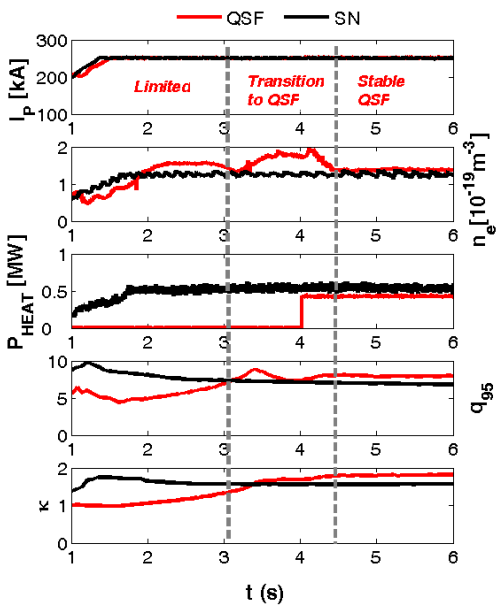


**Figure 10. Time evolution of main plasma quantities for SN (#47038) and QSF discharge (#48971): plasma current $I_P$, line avarage electron density $n_e$, additional heating $P_{HEAT}$ (LH and NBI power respectively for #47038 and #48971), $q_{95}$ and elongation $\kappa$. It should be noted that from ~4.3s the QSF configuration becomes stable.**

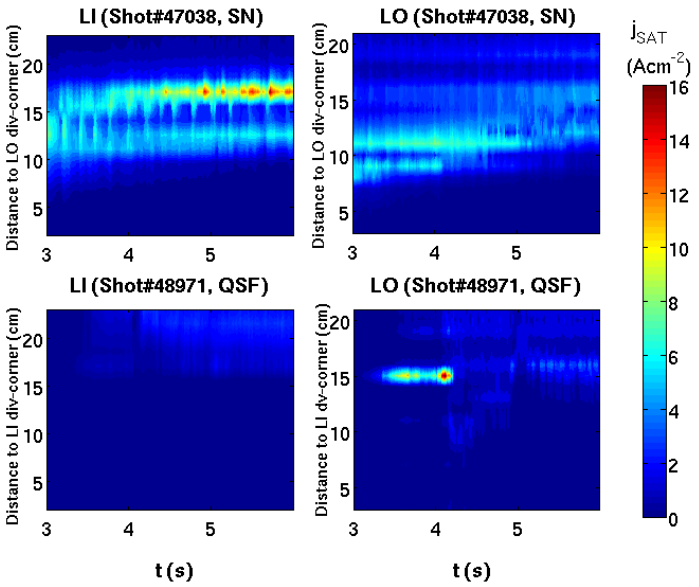


**Figure 11. Spatio-temporal profiles of the saturation current density $j_{SAT}$ for QSF and SN discharges. A first qualitative observation indicates that in discharge #48971, once QSF configuration becomes stable (i.e. after 4.3s, see Fig.12) the peak of $j_{SAT}$ on outer SP drastically drops. In SN discharge #47048, even if the particle fluxes to SPs are minor to QSF #48971, both inner and outer SPs are quite actived during all the discharge.**

Next experiments will be devoted to the verification of an adapted version of quasi-SF ISOFLUX shape controller and to H-mode discharges at low and high current, including a variation scan of the distance between the two x-points. Eventually, the final upgrade of the available additional power on EAST it will

allow to study the configurations up to a power flux ≈ 20MWm$^{-2}$, the very last limit compatible with the presently available materials.

# 4 References


1. Loarte A. et al 2007 Nucl. Fusion 47 S203
2. Eich T. et al 2011 Phys. Rev. Lett. 107 215001
3. Kotschenreuther M. et al 2007 Phys. Plasmas 14 72502
4. Valanju P.M. et al 2009 Phys. Plasmas 16 056110
5. Ryutov D.D. 2007 Phys. Plasmas 14 064502
6. Ryutov D.D. et al 2008 Phys. Plasmas 15 092501
7. Piras F. et al 2009 Plasma Phys. Control. Fusion 51 055009
8. Soukhanovskii V.A. et al 2011 J. Nucl. Mater. 415 S365–8
9. Allen S. et al 2012 proc. 24th Int. Conf. on Fusion Energy (San Diego, CA, 2012) and www-naweb.iaea.org/napc/physics/FEC/FEC2012/html/presenations/801 PD12.pdf
10. Wan Y. et al 2006 Overview progress and future plan of EAST Project Proc. 21th Int. Conf. on Fusion Energy 2006 (Chengdu, China 2006) (Vienna: IAEA) CD-ROM file OV/1-1 and www-naweb.iaea.org/napc/physics/fec/ fec2006/html/index.htmG. 1)
11. B.J. Xiao, et al, 2008 Fusion Eng. Des. 83 181-187
12. Ryutov D.D. et al 2012 Plasma Phys. Control. Fusion 54 124050.
13. Albanese R, Mattei M, Calabrò G and Villone F 2003 Unified treatment of forward and inverse problems in the numerical simulation of tokamak plasmas Proc. 11th Int. Symp. on Applied Electromagnetics and Mechanics (Versailles, France) pp 404–5
14. Lao L.L., et al., 1985 Nucl. Fusion 25 1611
15. Alladio F., Crisanti F., 1986 Nucl. Fusion 26 1143 (1986)
16. Guo Y., et al., 2012 Plasma Phys. Control. Fusion 54 085022
17. Albanese R., et al., Plasma Phys. Control. Fusion 2014 56 035008
18. Chen S.L., 2014 “Effect of three-dimensional conducting structures on vertical stability in EAST” submitted to Nucl. Fusion
19. R. Zagórski, H. Gerhauser, 2004 Physica Scripta 70, 173
20. Pericoli Ridolfini V., et al., 2007 Plasma Phys. Control. Fusion 49 S123
21. Pericoli Ridolfini V.. et al., 2013 J. Nucl. Mat. 438 S414
22. Pericoli Ridolfini V., et al., 2013 Fus. Eng. Des. 88 167
23. R. Simonini, et al. Contrib. Plasma Phys. 34, 368 (1994)
24. Xiao, B.J., et al., 2012 Fusion Eng. Des 87 1887

# 5 Abbreviations and acronyms

| | |
|---|---|
| 3D | three Dimensional |
| CAD | Computer Aided Design |
| EM | Electro-Magnetic |
| FEM | Finite Elements Model |
| FW | First Wall |
| MHD | Magneto Hydro Dynamics |
| PC | Plasma Chamber |
| PF | Poloidal Field |
| RH | Remote Handling |
| SF | Snow Flake |
| SN | Single Null |
| SX | Super-X |
| TF | Toroidal Field |
| VV | Vacuum Vessel |